Chromium Poisoning of $La_{1-x}Sr_xMnO_{3\pm\delta}$ Cathodes and Electrochemical Validation of Chromium Getters in Intermediate Temperature-Solid Oxide Fuel Cells

Su Jeong Heo,[1,2] Junsung Hong,[1] Ashish Aphale,[1] Boxun Hu,[1] and Prabhakar Singh[1,z]

[1]*Department of Materials Science and Engineering, University of Connecticut, Storrs, Connecticut 06269, USA*
[2]*Materials Science Center, National Renewable Energy Laboratory, Golden, Colorado 80401, USA*

The effect of chromium poisoning on electrochemical performance degradation has been studied at intermediate temperatures (550–650°C) using $La_{1-x}Sr_xMnO_{3\pm\delta}$ (LSM) cathode and an electrochemical cell configuration air/LSM//YSZ//Pt/air. A rapid increase in polarization resistance is observed in the presence of gaseous chromium species containing humid air (3% H_2O) at both 550°C and 650°C. Cross-sectional elemental mapping and high-resolution transmission electron microscopy of the LSM/YSZ interface show the presence of crystalline Cr_2O_3 and $(Mn,Cr)_3O_4$ phases indicating reduction of gaseous hexavalent-chromium species and deposition of solid reaction products. Subsequent experiments, performed under the above exposure conditions but in the presence of a chromium getter, showed stable polarization resistance. The electrochemical performance of half-cells in Cr-containing humid air atmosphere and in the presence of the chromium getter also remained stable during 100-h tests at 550 and 650°C, respectively. The post-test structural and chemical analysis of the electrode, electrode-electrolyte interface and getter by scanning- transmission electron microscopy, energy dispersive X-ray and Raman spectroscopy showed that the cathode bulk and cathode- electrolyte interface remained free of chromium deposits whereas chromium species deposited near the air inlet region of the porous getter as crystalline $SrCrO_4$.

 [DOI: 10.1149/2.0931913jes]

Manuscript submitted June 25, 2019; revised manuscript received August 18, 2019. Published August 28, 2019.

Typical long term operation of solid oxide fuel cells (SOFC) at high temperatures (800–1000C) allows high energy conversion efficiency and integration with gas turbines for large-scale stationary applications.[1–3] but imposes significant constraints on cell, stack and balance of plant materials due to solid-solid and solid-gas interactions. In recent years, significant progress has been made toward the development of SOFCs capable of operating efficiently at intermediate temperature (550–750°C) for small and distributed scale applications.[4–6] Lowering the operating temperature allows the use of conventional low cost metallic and ceramic materials as well as provides an opportunity for the selection of stack and balance of plant (BoP) component materials for further cost reduction (materials and processing cost), use of conventional and emerging large-scale fabrication techniques.

To date, chromia-forming stainless steels are the leading IC and BoP materials of choice for planar SOFCs due to desired electrical/thermal conductivity, mechanical properties, and oxidation/corrosion resistance.[7,8] Chromia scale formed on the above alloy surfaces, however, reacts with oxygen and water vapor(H_2O) present in air and generates volatile chromium-containing species such as CrO_3, $CrO(OH)_2$, and $CrO_2(OH)_2$ under the SOFC[9,10] operating conditions. Interaction of the above volatile chromium species with the cathode leads to irreversible performance degradation due to increase in the cathodic polarization and charge-transfer resistances, compound formation and coverage of triple-phase boundaries.[11,12] While Sr doped predominantly electronically conducting lanthanum manganite [LSM $(La,Sr)MnO_3$)] remains prone to chromium poisoning due to the formation of Cr_2O_3 and $(Mn,Cr)_3O_4$ at electrochemically active triple phase boundaries, mixed conducting Sr and Fe doped lanthanum cobaltite [LSCF $(La,Sr)(Co,Fe)O_3$] indicate surface coverage and formation of $SrCrO_4$ on the free surface rather than the electrochemically active triple-phase boundaries primarily due to the interactions with segregated SrO and gaseous Cr species.[13–15]

The partial pressure of gaseous chromium species has been calculated and found to largely depend on the humidity level (steam content or pressure) in air. Chen et al.[16] reported the effect of Cr deposition and poisoning of the LSM cathode in humidified air to be significant as compared to that in dry air due to the higher concentration of the $CrO_2(OH)_2$ gaseous species. Gindorf et al.[17] studied Cr vaporization from Cr_2O_3 powder and reported significant increase in evaporation rate with increasing temperature and humidity conditions. Although Cr evaporation is considered to be suppressed at intermediate temperatures, gaseous chromium species are still amenable for deposition on the free cathode surface and interface between cathode and electrolyte.[18,19] The influence of chromium species on the cathodic degradation at intermediate temperatures, hence, need further investigation.

To mitigate Cr assisted electrochemical poisoning of the cathode, the use of Cr getters has been considered. Strontium nickel oxide (SNO) has been used as the getter material and its thermal and hydrolytic stability has been studied.[20,21] Although excellent capability of the getter for capturing Cr species at high temperature (850°C) has been demonstrated experimentally using electrochemical techniques,[22] getter's Cr capturing performance at intermediate temperatures (500–700°C) remains unknown.

In this research article, we have studied Cr poisoning of the LSM electrode and the role of Cr getter at intermediate temperatures (550–650°C). Electrochemical tests were conducted in the presence and the absence of the getter composed of strontium nickel oxide at 550°C and 650°C. Bulk LSM, LSM/YSZ interface and the getter have been characterized using scanning- transmission electron microscopy, energy dispersive X-ray and Raman spectroscopy to elucidate Cr poisoning mechanism and the efficacy of the getter for the capture of Cr at intermediate temperatures.

Experimental

Cell fabrication.—Lanthanum Strontium Manganite ink ($(La_{0.80}Sr_{0.20})_{0.95}MnO_{3-x}$, FuelCell Materials) was mixed with vehicle ink (FuelCell Materials) to form the electrode ink and then screen printed onto the surface of YSZ button substrate (8 mole % yttria, 0.25–0.30 mm thick, FuelCell Materials) as reported in our earlier report.[23] The fabricated half-cells were subsequently sintered at 1200°C in ambient air for 2 hours with a ramp rate of 3°C min^{-1}. Platinum electrodes were used as anode to eliminate the possibility of the anode delamination from the electrolyte surface.[24] Platinum paste (ESL Electroscience) was subsequently painted to attach platinum gauzes and wires (Alfa Aesar) together on the cathode and anode electrodes and cured in air at 850°C for 1 hour at a ramp rate of 3°C min^{-1}. Platinum wires were also attached on the YSZ substrate as a reference current collector.

[z]E-mail: prabhakar.singh@uconn.edu

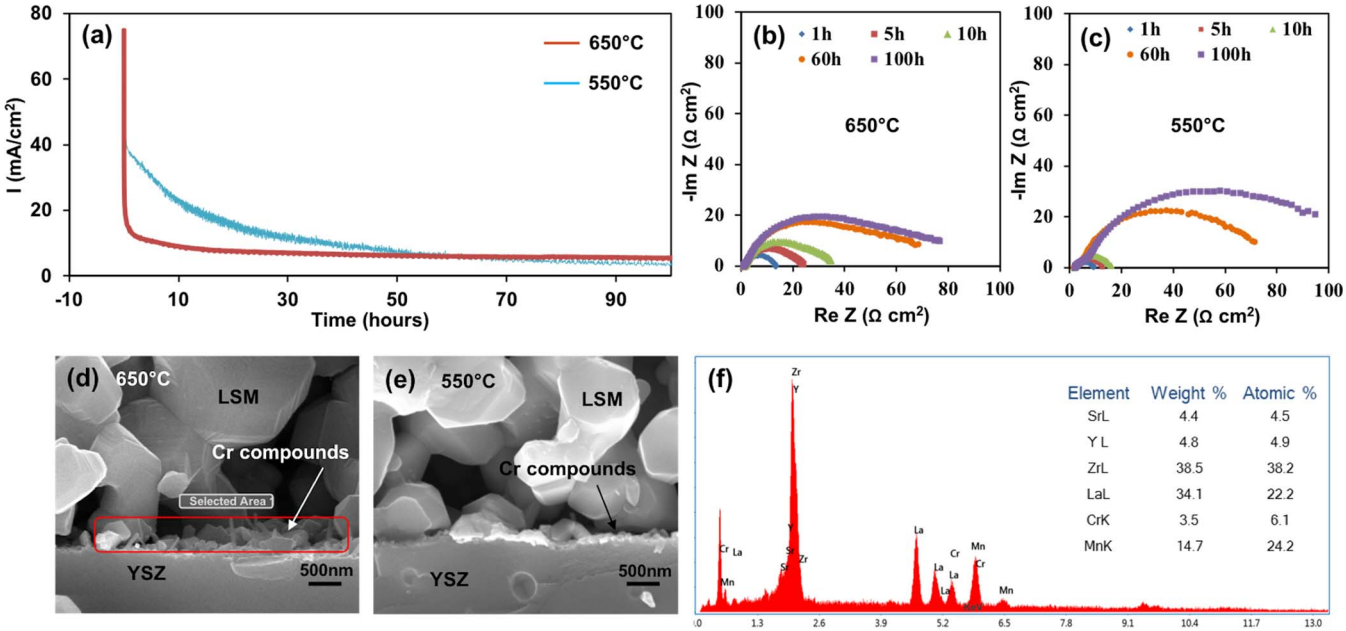

Figure 1. (a) Electrochemical performance (I-t curve) and impedance spectra of the half-cell in the presence of Cr vapors at (b) 650°C and (c) 550°C. SEM images of the cross-sections of the LSM/YSZ interface after the test in 3% H_2O/air in the presence of Cr vapor at (d) 650°C and (e) 550°C, and (f) EDS spectrum at the LSM/YSZ interface in Figure 1d (marked by a red box).

Electrochemical testing.—Electrochemical tests using half-cell configuration (Air/LSM//YSZ//Pt/Air) were performed to evaluate the gaseous chromium vapor assisted poisoning and the effectiveness of the getter at 550°C and 650°C. assembled half-cells were tested in humidified (3%H_2O) air in the presence of a Cr source for 100 hours. To evaluate the effect of SNO getter for capturing the chromium species, similar test configuration was used for placing the SNO getter between the chromium source and the cathode as shown in Figure 6 (right panel). Baseline experiments on the half-cell in chromium-free humidified air were performed without the getter as a reference for comparison (baseline). Time-dependent electrochemical impedance spectra (EIS, Bio-Logic) were obtained to analyze the changes in the half-cell electrode polarization at an applied bias of 0.5 V in the frequency range of 0.5 Hz to 200 kHz with a 10 mV sinus amplitude at an interval of 1 h.

Getter fabrication.—Strontium nitrate ($Sr(NO_3)_2$) (Sigma-Aldrich) and nickel nitrate ($Ni(NO_3)_2.6H_2O$) (Sigma-Aldrich) (49:51 mol.%) were dissolved in DI water at 80°C. Ammonium hydroxide was slowly added to the aqueous solution until pH became 8.5. The solution was dried for 24 h in a drying oven and the dry powder was rinsed out with DI water to remove any ammonium nitrate present in the product. The resultant powder was mixed with DI water to prepare an aqueous slurry. Al_2O_3 microfibers-based substrates (Zircar) with cylindrical shape were selected for the coating of the getter material. The substrate was submerged in the slurry followed by drying for 24 h and heat-treatment in air at 650°C for 4 hours to obtain $S_xN_yO_z$ getter.

Characterization.—The morphological and elemental analyses were conducted using an FEI Quanta 250 FEG scanning electron microscopy (SEM) with a field emission source equipped with an Everhart-Thornley SE (secondary electron) detector and an energy-dispersive X-ray spectroscopy (EDS). The sample for transmission electron microscopy (TEM) analysis was prepared by a focused ion beam (FIB) instrument (FEI Strata 400s Dual Beam FIB), combined with a scanning electron beam and an ion beam. The dual-beam gives high-resolution imaging of the sample with the ion-beam milling. TEM studies were performed using JEOL JEM-2010 FasTEM. Raman spectra were recorded with Renishaw System 2000 using a 514 nm excitation line.

Results and Discussion

Chromium poisoning at intermediate temperatures.—The effect of chromium poisoning on Air/LSM//YSZ//Pt/Air half-cells has been examined using a number of repeat electrochemical tests performed at 550°C and 650°C, respectively. As shown in Figure 1a, with a constant bias of 0.5 V, the cell current decayed rapidly in the presence of Cr vapor at both 650°C and 550°C. The Nyquist impedance semicircles diameter (Figures 1b and 1c) increased over time, indicating an increase in the polarization resistance. In particular, the polarization resistance significantly increased after the first 10-hour exposure (attributed to the deposition of Cr species on the electroactive sites in the cathode).

The cathode/electrolyte interface morphology of the tested cell was examined by SEM. Formation of secondary phases is observed at the LSM/YSZ interface for cells tested in the presence of Cr vapor at both 650°C (Figure 1d) and 550°C (Figure 1e). Elemental analysis (Figure 1f) of the selected area in Figure 1d indicates the presence of chromium ($\sim$ 6 at. %).

A thin specimen of post tested cell was prepared by focused ion beam (FIB). Analysis by electron diffraction spectroscopy (Figure 2) shows the presence of Cr deposits at the LSM electrode and YSZ electrolyte interface.

Analysis of chromium-rich layer (the region of yellow rectangle box in Figure 2) was performed by TEM to identify the chromium compounds (Figure 3). Figures $3a_2$ and $3b_2$ show high-resolution TEM images with clear crystalline lattice fringes. The fringes are indexed according to the generated fast Fourier transform (FFT) patterns (Figures $3a_3$ and $3b_3$). Figure 3a shows that the fringe spacing of 0.23 nm corresponds to the {006} planes, while the fringe spacing of 0.36 nm corresponds to the {112} planes of rhombohedral Cr_2O_3, with space group, $R\bar{3}c$, (no. 167), a = 4.960 Å and c = 13.598 Å. The angle between (006) and (112) in both the HRTEM and FFT images is calculated to be 57°, which is identical to the theoretical value of the angle between the {006} and {012} facets as observed in the atomic model

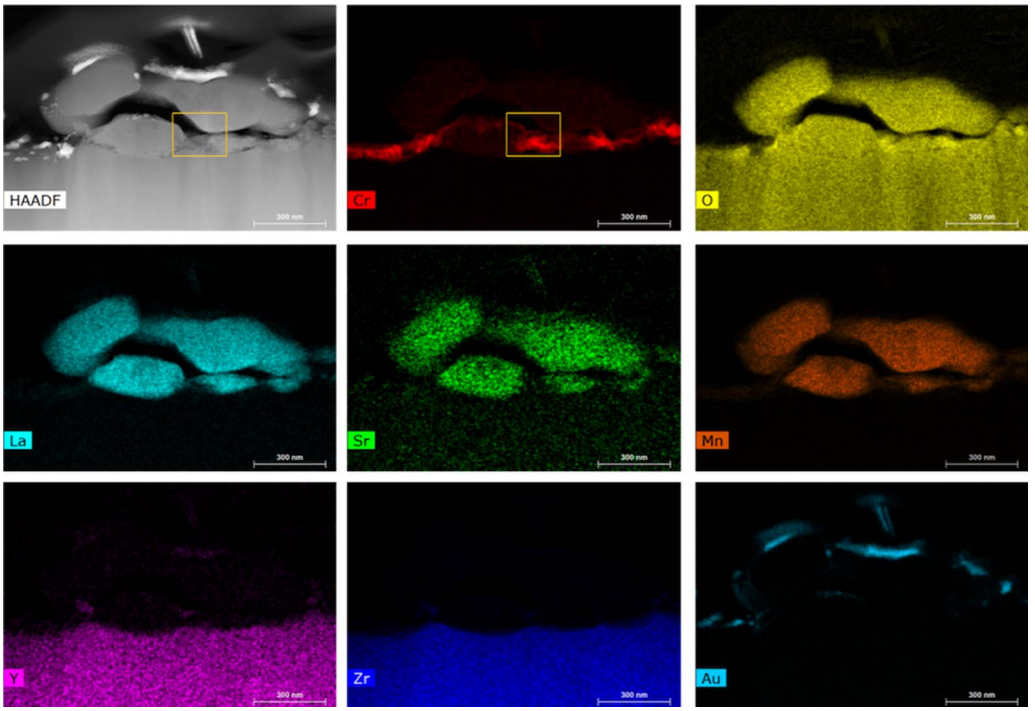

Figure 2. STEM micrograph and EDS mapping on the cross-section of the LSM electrode/YSZ electrolyte interface after the test in the presence of Cr vapor at 650°C in 3%H_2O-air for 100 h.

of rhombohedral Cr_2O_3 (Figure 3a$_4$). The TEM results (Figure 3b) suggest that the crystalline pattern matches with spinel $(Mn,Cr)_3O_4$, which is the space group of $I4_1/amd$ (no. 141) with the lattice parameter of $a = 5.9060$ Å and $c = 8.7650$ Å. The 121° angle between (022) and (211) is matched with the theoretical value as shown in the atomic model of spinel $(Mn,Cr)_3O_4$ as shown in Figure 3b$_4$.

Our observations validate the formation of solid Cr_2O_3 and $(Mn,Cr)_3O_4$ at the LSM/YSZ interfaces when the electrochemical testing was conducted in the presence of Cr vapor in 3% H_2O/air, even at lower operating temperatures. Figure 4a shows the partial pressures of Cr vapors calculated from thermochemical database (HSC Chemistry 6.12, Outotec Oyj, Finland) and compared to those calculated by Chen[16] and Hilpert.[25] Although the HSC database show relatively lower partial pressures of gaseous chromium species when compared to other reported data, the trend remains similar. The most abundant Cr vapor species in humid air is $CrO_2(OH)_2$ and CrO_3 in dry air. We

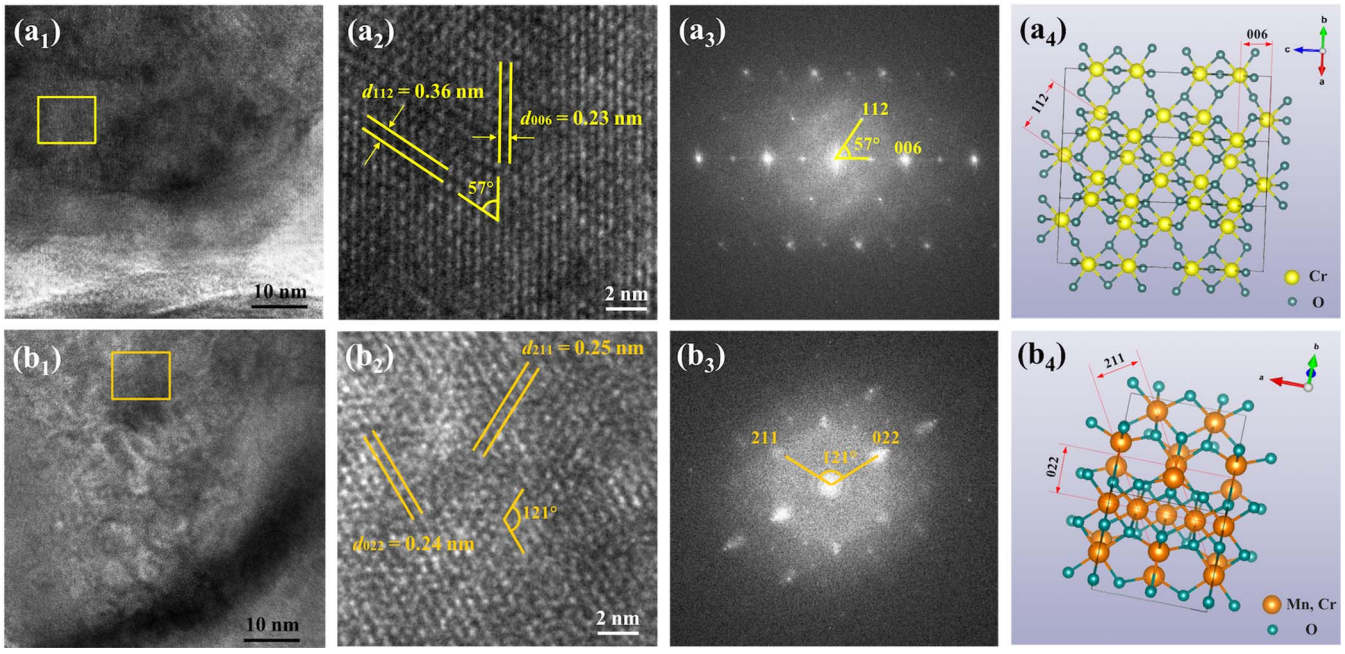

Figure 3. TEM images of the chromium species deposited at the cathode interface taken along (a_1) [110] and (b_1) [011]. High-resolution TEM images of the crystallites (a_2 and b_2) of the rectangle region in a_1 and b_1 and the corresponding Fourier transform pattern (a_3 and b_3) are matched well with the atomic model of rhombohedral Cr_2O_3 (a_4) and spinel $(Mn,Cr)_3O_4$ (b_4) illustrated, respectively.

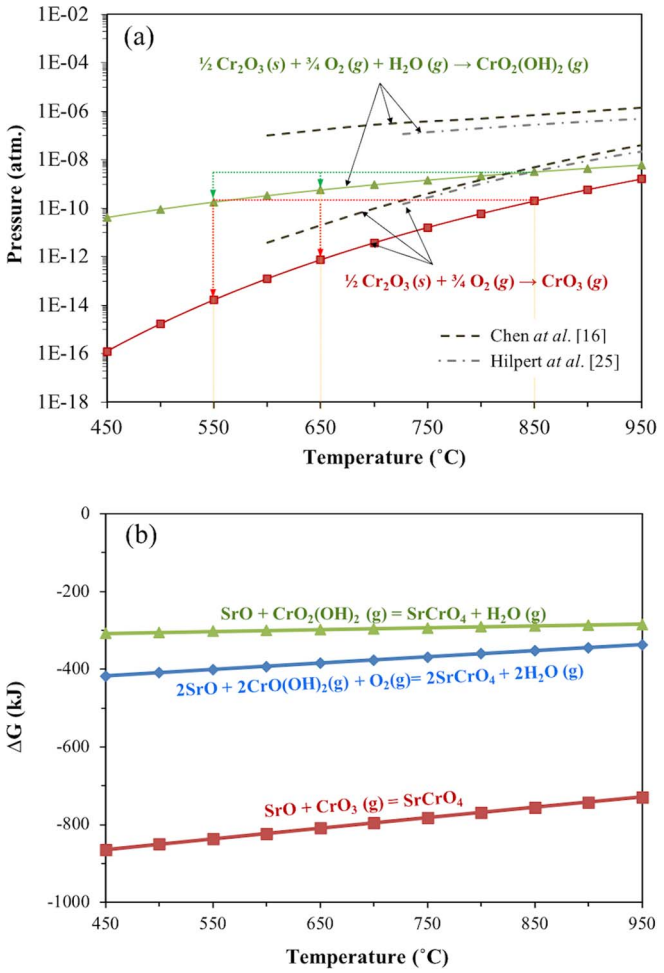

Figure 4. (a) Partial pressures of gaseous chromium species in the humidified air (3%H_2O) and dry air as a function of temperature and compared to those calculated by Chen[16] and Hilpert.[25] (b) Gibbs free energies for the formation of $SrCrO_4$ as a function of temperature.

note that the partial pressure of gaseous CrO_3 is significantly reduced at lower temperatures as indicated by larger slope while the gaseous $CrO_2(OH)_2$ partial pressure remains relatively high at lower temperatures as indicated by smaller slope suggesting that the available Cr vapor remains a concern for the electrode poisoning in lower temperature SOFC systems.

Formation of Cr_2O_3 and $(Mn,Cr)_3O_4$ is attributed to interactions between the cathode and gaseous $CrO_2(OH)_2$ rather than CrO_3 at lower temperatures and that the chromium oxides are deposited at the LSM/YSZ interface rather than the LSM surface due to (a) reduction of Cr^{6+} to Cr^{3+}, (b) absence of surface SrO deposit on LSM and (c) electronic conductivity of LSM. It is further suggested that LSM is locally reduced remaining oxygen-deficient under cathodic polarization. The formation of oxygen vacancies is compensated by partial reduction of Mn^{3+} to Mn^{2+}.[26] Since Mn^{2+} ions generated are mobile, it migrates onto the YSZ electrolyte surface and eventually reduces the gaseous chromium to Cr_2O_3 and $(Mn,Cr)_3O_4$ at the triple-phase boundaries through the reactions.[27,28]

$$CrO_2(OH)_2(g) + Mn^{2+} + e^- \rightarrow Cr - Mn{-}O_{nucleus} + H_2O(g) \quad [1]$$

$$CrO_2(OH)_2(g) + Cr - Mn{-}O_{nucleus} \rightarrow (Cr, Mn)_3O_4(s) + H_2O(g) \quad [2]$$

$$CrO_2(OH)_2(g) + 3e^- \rightarrow \frac{1}{2}Cr_2O_3(s) + H_2O(g) + \frac{3}{2}O^{2-} \quad [3]$$

Mitigation of electrochemical degradation.—The effectiveness of the developed getter to capture the gaseous Cr species has been experimentally validated using electrochemical test setup shown in Figure 5. SrO has been considered as an active getter constituent for the capture of Cr vapor species such as $CrO_2(OH)_2$, $CrO(OH)_2$, and CrO_3 to form thermodynamically stable solid $SrCrO_4$. The calculated free energy change (ΔG) for the above interactions involving SrO and gaseous chromium species for the formation of solid $SrCrO_4$ remains negative and thus favorable as shown in Figure 4b.

$$SrO(s) + CrO_2(OH)_2(g) \rightarrow SrCrO_4(s) + H_2O(g) \quad [4]$$

$$SrO(s) + CrO(OH)_2(g) + 1/2\,O_2(g) \rightarrow SrCrO_4(s) + H_2O(g) \quad [5]$$

$$SrO(s) + CrO_3(g) \rightarrow SrCrO_4(s) \quad [6]$$

Solid solutions of SrO with transition metal oxides such as NiO has been further considered for potential getter formulation due to its observed structural and chemical instabilities of SrO due to the formation of hydroxides and carbonates that can also result in volume expansion and delamination of the getter layer from supporting substrates. We have developed $Sr_xNi_yO_z$ (SNO) powder as an alternate material (with lower SrO activity and resistance to hydration and carbonation), which is thermally stable up to 950°C.[20,21] The getter was installed in the air inlet stream ahead of the electrochemical cell to capture the incoming chromium vapor as shown in Figure 6 (top right).

Figure 5a shows the electrochemical half-cell performance in the presence of Cr vapor at 650°C. Compared to the degradation of the cell performance in the presence of Cr vapor within a few hours, both cells with Cr vapor/getter and without Cr vapor/getter (baseline) show stable performance for over 100 hours during electrochemical tests. The EIS measurements also show no significant change ion electrode polarizations over time when the getter was placed between the cathode and the Cr source. The above trend also remains similar to that observed during the baseline test indicating that the cathode remained stable due to the capturing of the Cr vapor by getter and keeping the cell electrode polarization stable. The cell performance trend appeared identical for the electrochemical test conducted at 550°C, thus confirming the beneficial effect of the Cr getter at intermediate temperatures.

Figure 6 shows the chromium distribution along the air flow direction in the getter channel as measured by SEM-EDS after the completion of electrochemical test at 650°C. The region of getter inlet (Figure 6b, red rectangle) shows the chromium deposition on the inlet getter surface. The chromium concentration is significantly reduced from 12.6 at% (at the inlet) to 0–1.5 at% in the middle and outlet of the getter indicating that the chromium vapor is largely captured at the inlet (approximately in 2.5 mm). Figure 6 shows Raman spectra of the inlet side of the getter exposed to Cr vapor at 550°C and 650°C during the electrochemical test. The Raman bands at 860, 889, 375, and 402 cm^{-1} correspond to $SrCrO_4$ phase.[29] The most dominant chromium vapor species, $CrO_2(OH)_2$, formed in humidified air as well as other prevalent gaseous species ($CrO(OH)_2$ and CrO_3) readily reacted with SrO present in SNO to form stable $SrCrO_4$. Consequently, chromium species do not deposit on the LSM/YSZ interface and the electrical performance remains stable even under chromium vapor (Figure 7).

Conclusions

Chromium poisoning of LSM cathode has been studied at intermediate SOFC operating temperatures. In the presence of Cr vapors, the electrochemical performance of the cathode rapidly degraded due to an increase in the electrode polarization resistance. Posttest cross-sectional analysis identified the presence of Cr species as Cr_2O_3 and $(Mn,Cr)_3O_4$ phases at the LSM/YSZ interface. The Cr getters composed of $Sr_xNi_yO_z$ were subsequently utilized to capture gaseous chromium vapors. In the presence of the getter, the electrode performance remained stable with no change in the polarization resistance during the 100 hours electrochemical test. While the getter captured

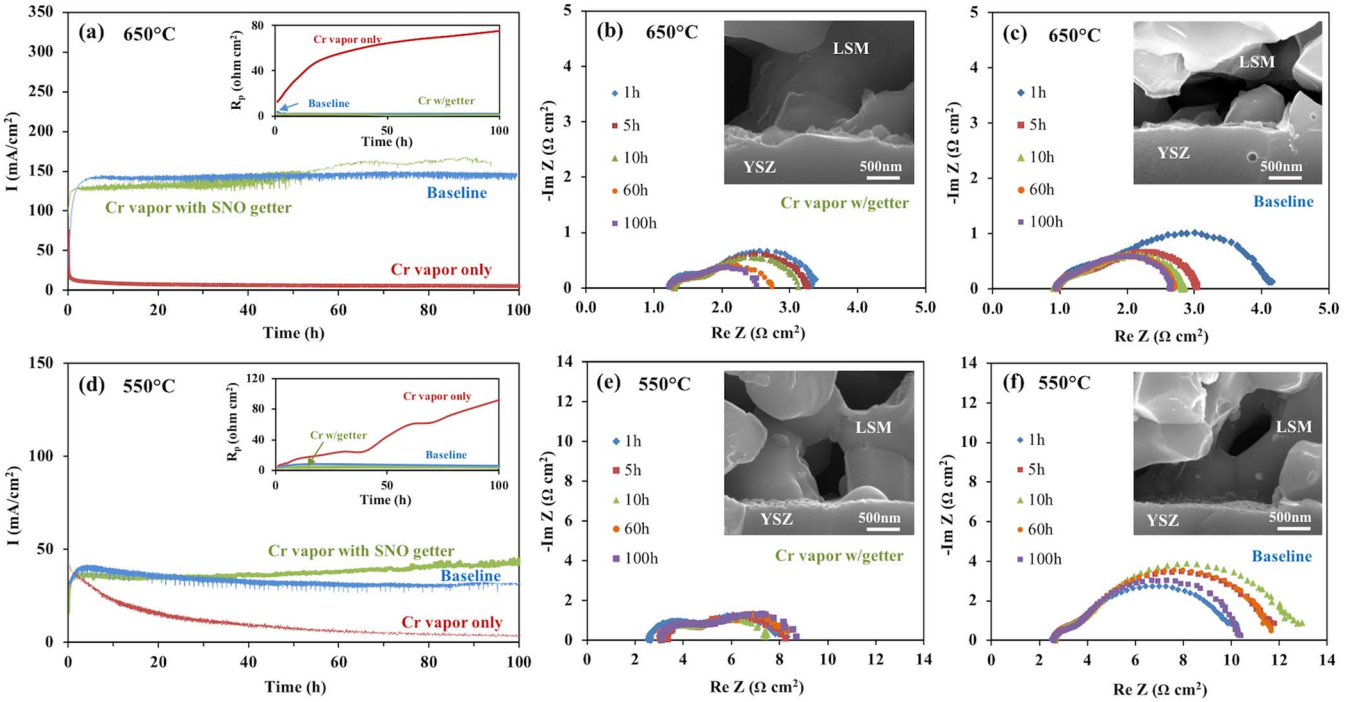

Figure 5. Comparison of I-time curves (a and d) and Rp-time plots (inserted in a and b) of the three half-cell tests at 650°C and 550°C, respectively. Impedance spectra of the cells of getter with Cr vapor (b and e) and baseline test (c and f) at 650°C and 550°C, respectively. SEM images of fracture areas are inserted in the boxes of each Nyquist spectra.

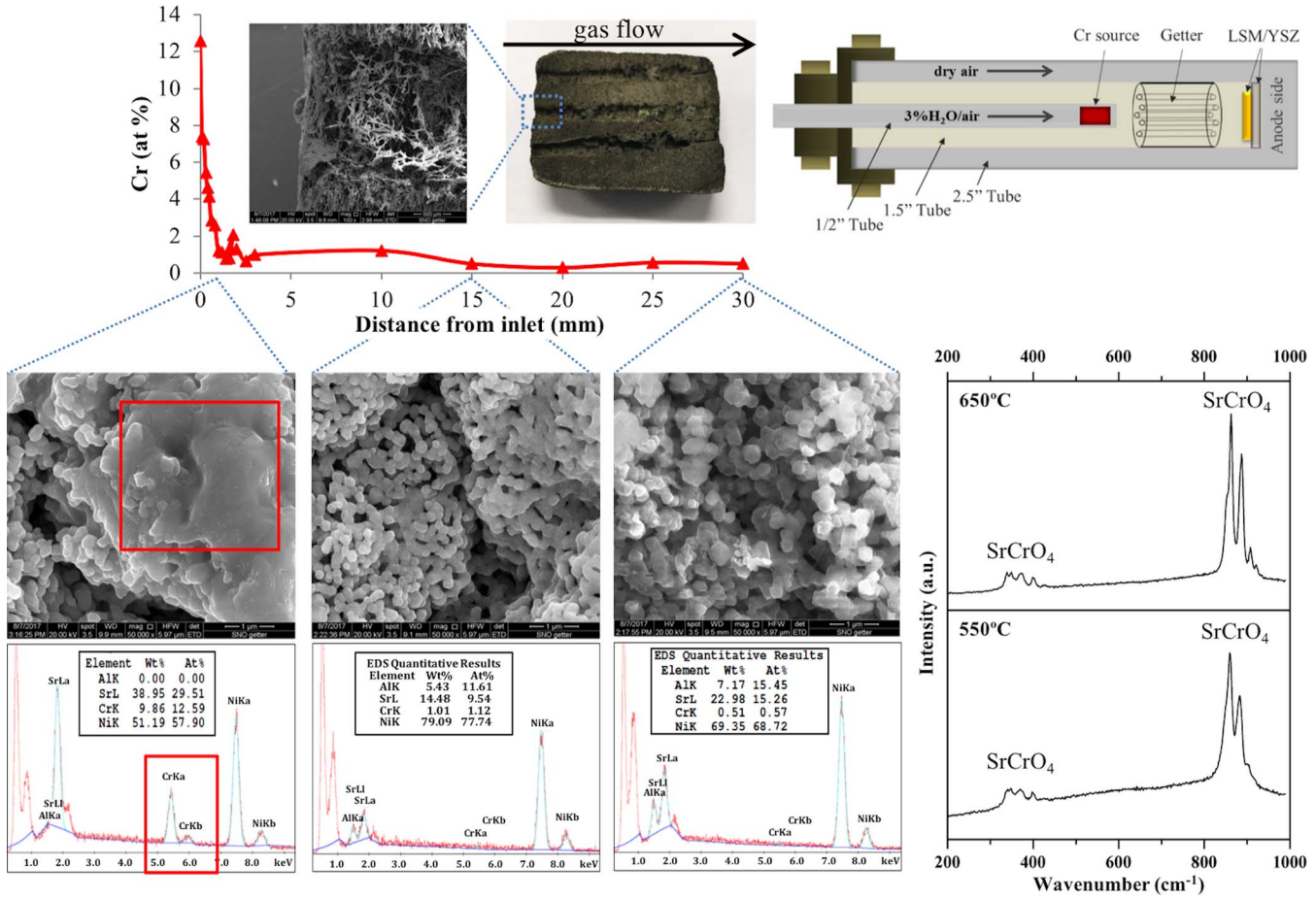

Figure 6. Chromium distributions across the getter inlet, middle, and outlet measured by SEM-EDS (left). Schematic of the electrochemical test setup for the half-cell in the presence of Cr source and chromium getter (right above). Raman spectra of the getter inlet region (right below).

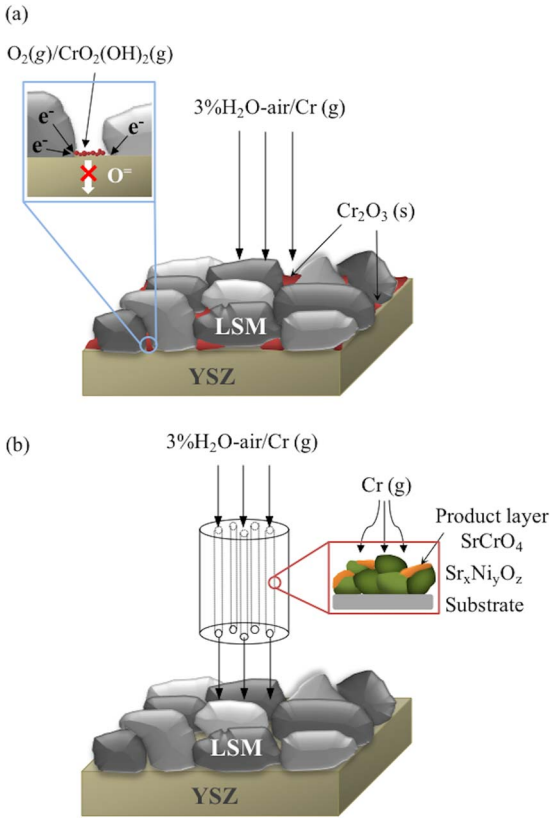

Figure 7. Illustration of chromium deposition on (a) the LSM/LSZ interface and (b) the effect of the SNO getter mitigating the electrochemical degradation.

gaseous chromium species at the air inlet, the electrode remained free of chromium.

Acknowledgments

Authors acknowledge financial support from the US Department of Energy and National Energy Technological Laboratory under federal grant DE-FE 0023385. Technical discussions with Dr. Jeff Stevenson is acknowledged. We thank Center for Clean Energy Engineering, University of Connecticut for providing the instrument and facilities for the timely completion of experiments.

ORCID

Junsung Hong https://orcid.org/0000-0003-2238-532X

References

1. S. R. Bishop, X. Liu, and A. Aguadero, *J. Electrochem. Soc.*, **164** (10), Y11 (2017).
2. A. J. Jacobson, *Chem. Mater*, **22**, 660 (2010).
3. J. Wu and X. Liu, *J. Mater. Sci. Technol.*, **26**(4), 293, (2010).
4. D. J. L. Brett, A. Atkinson, N. P. Brandon, and S. J. Skinner, *Chem. Soc. Rev.*, **37**, 1568 (2018).
5. Z. Gao, L. V. Mogni, E. C. Miller, J. G. Railsback, and S. A. Barnett, *Energy Environ. Sci.*, **9**, 1602 (2016).
6. E. D. Wachsman and K. T. Lee, *Science*, **334**, 935 (2011).
7. J. A. Schuler, C. Gehrig, Z. Wuillemin, A. J. Schuler, J. Wochele, C. Ludwig, A. Hessler-Wyser, and J. V. Herle, *J. Power Sources*, **196**(17), 7225 (2011).
8. P. Singh, *Am. Ceram. Soc. Bull.*, **95**(2), 16 (2016).
9. B. Huang, X.-J. Zhu, R.-X. Ren, Y.-X Hu, X.-Y. Ding, Y.-B Liu, and Z.-Y. Liu, *J. Power Sources*, **216**, 89 (2012).
10. R. Wang, M. Wurth, U. B. Pal, S. Gopalan, and S. N. Basu, *J. Power Sources*, **360**, 87 (2017).
11. N. H. Menzler, D. Sebold, and Q. Fang, *J. Electrochem. Soc.*, **162**(12), F1275 (2015).
12. E. Park, S. Taniguchi, T. Daio, J.-T. Chou, and K. Sasaki, *Solid State Ionics*, **262**, 421 (2014).
13. R. A. Budiman, K. D. Bagarinao, S. S. Liu, D. H. Cho, T. Ishiyama, H. Kishimoto, K. Yamaji, T. Horita, and H. Yokokawa, *J. Electrochem. Soc.*, **165**(14), F1206 (2018).
14. L. Zhao, J. Drennan, C. Kong, S. Amarasinghe, and S. P. Jiang, *J. Mater. Chem. A*, **2**, 11114 (2014).
15. B. Hu, S. Krishnan, C. Liang, S. J. Heo, A. N. Aphale, R. Ramprasad, and P. Singh, *Int. J. Hydrogen Energy*, **42**, 10208 (2017).
16. X. Chen, Y. Zhen, J. Li, and S. P. Jiang, *Int. J. Hydrogen Energy*, **35**, 2477 (2010).
17. C. Gindorf, L. Singheiser, and K. Hilpert, *J. Phys. Chem. Solids*, **66**, 384 (2005).
18. H. Falk-Windisch, J. E. Svensson, and J. Froitzheim, *J. Power Sources*, **287**, 25 (2015).
19. S. Taniguchi, M. kadowaki, H. Kawamura, T. Yasuo, Y. Akiyama, Y. Miyake, and T. Saitoh, *J. Power Sources*, **55**, 73 (1995).
20. J. Hong, S. J. Heo, A. N. Aphale, B. Hu, and P. Singh, *J. Electrochem. Soc.*, **166**(2), F59 (2019).
21. A. Aphale, M. A. Uddin, B. Hu, S. J. Heo, J. Hong, and P. Singh, *J. Electrochem. Soc.*, **165**(9), F635 (2018).
22. A. Aphale, J. Hong, B. Hu, and P. Singh, *J. Vis. Exp.*, **147**, e59623 (2019).
23. B. Hu, M. Keane, M. K. Mahapatra, and P. Singh, *J. Power Sources*, **248**, 196 (2014).
24. M. Keane, M. K. Mahapatra, A. Verma, and P. Singh, *Int. J. Hydrogen Energy*, **37**, 16776 (2012).
25. K. Hilpert, D. Das, M. Miller, D. H. Peck, and R. Wei, *J. Electrochem. Soc.*, **143**(11), 3642 (1996).
26. A.-K. Huber, M. Falk, M. Rohnke, B. Luerssen, M. Amati, L. Gregoratti, D. Hesse, and J. Janke, *J. Catal.*, **294**, 79 (2012).
27. S. P. Jiang, J. P. Zhang, L. Apateanu, and K. Foger, *J. Electrochem. Soc.*, **147**(11) 4013 (2000).
28. J. A. Schuler, H. Yokokawa, C. F. Calderone, Q. Jeangros, Z. Wuillemin, A. Hessler-Wyser, and J. V. Herle, *J. Powder Sources*, **201**, 112 (2012).
29. L. Zhao, J. Zhang, T. Becker, and S. P. Jiang, *J. Electrochem. Soc.*, **161**(6) F687 (2014).